Hindawi
Wireless Communications and Mobile Computing
Volume 2023, Article ID 3069999, 14 pages
https://doi.org/10.1155/2023/3069999

Research Article

SWIPT-Based Cooperative NOMA for Two-Way Relay Communications: PSR versus TSR

Huu Q. Tran[1] **and Quoc-Tuan Vien**[2]

[1]*Industrial University of Ho Chi Minh City, Vietnam*
[2]*Middlesex University, UK*

Correspondence should be addressed to Huu Q. Tran; tranquyhuu@iuh.edu.vn

Received 5 August 2022; Revised 23 October 2022; Accepted 7 January 2023; Published 17 January 2023

Academic Editor: Zhengyu Zhu

Spectrum and energy efficiency with simultaneous wireless information and power transfer (SWIPT) to prolong the lifetime of power-constrained wireless devices in cooperative relaying nonorthogonal multiple access (CR-NOMA) has received great attention in the last decade. This paper investigates a two-way relay channel in a CR-NOMA system where two users exchange data with the assistance of a relay. Power-splitting relaying (PSR) and time-switching relaying (TSR) protocols are employed at the relay to harvest RF energy and process information from two users. We firstly derive the exact expressions of outage probability (OP) and system throughput (ST). The impacts of signal quality, energy coefficients, the distance of the nodes, and the data rate of two users on these performance metrics are then evaluated through several system settings to reflect practical network scenarios. It is shown that the OP and ST of the TSR are superior to that of the PSR protocol. Specifically, numerical results indicate that a higher throughput of up to 8% can be achieved with the TSR when compared to the PSR. It is further revealed that the OP and ST of the PSR are strongly affected by energy harvesting (EH) coefficients, while the performance obtained with the TSR is nearly independent of the EH capability at the relay.

1. Introduction

The introduction of the nonorthogonal multiple access (NOMA) concept to enhance spectrum efficiency, system throughput, latency, and user fairness has smoothed the path to the development of 5G wireless communication networks [1]. These crucial characteristics are limited in the traditional orthogonal multiple access (OMA) over either time or frequency domain. A variety of NOMA forms have been studied by many research groups [2, 3] among which power-domain NOMA (PD-NOMA) allows multiple users to be served in the same frequency and time resources but still ensures user fairness. In the PD-NOMA, the far-end user with poor channel conditions is allocated more power than the near-end user who experiences much better channel conditions [4]. At the transmitter, the signals of all users are combined using the superimposed coding (SC) technique. This combined signal is then sequentially decoded at the receivers using a successive interference cancellation (SIC) mechanism [5–8].

Inspired by the advantages of the PD-NOMA technique, cooperative relaying NOMA (CR-NOMA) has been developed to broaden the coverage region of radio frequency (RF) waves of the source and increase the integrity of the signal [9–12]. In the CR-NOMA, the far-end user is generally assumed that it cannot directly receive the transmit signal from the source due to physical obstacles or far distance. Thus, to ensure the transmit signal from the source can reach this user, a near-end user acts as a one-way relay to forward the signal to the far end in one direction [13]. The CR-NOMA has been extended for two-way relay networks (TWRNs) [12–14] that allow two users to exchange their information via a relay employing multiple antennas. In [15], the outage performance of a TWRN was evaluated based on a relay selection scheme. The performance in terms of outage probability (OP) and ergodic rate of the two-way

relay NOMA systems was derived for both perfect and imperfect SIC as well as the existence of an eavesdropper [11, 12].

1.1. Related Works. The energy in wireless devices is always constrained by the limited battery supply power. To prolong their lifetime, several solutions have been studied to combat the energy inefficiency problem as well as to provide green and effective communications [16]. In particular, over wireless media, RF signals can carry both energy and information. Such a useful endless energy source can be exploited to provide a supplementary power supply in wireless communication systems. In CR-NOMA, simultaneous wireless information and power transfer (SWIPT) [11, 17, 18] techniques can be employed for simultaneous energy harvesting (EH) and information processing (IP) at the relays. Power splitting- (PS-) and time switching- (TS-) based SWIPT is commonly exploited in receiver designs for EH and IP in wireless networks [19]. In the PS technique, the received power is split into two parts in which one is for the IP and the other is for the EH. In contrast, the TS technique performs switching the received signal between the EH and the IP. Recently, wireless-powered communications in TWRN have received great attention [13, 16, 20]. The authors in [13] proposed a novel full-duplex cooperative nonorthogonal multiple access (FD CNOMA) system in which a decode-and-forward- (DF-) based two-way relay was exploited in delay-limited transmission (DLT) and delay-tolerant transmission (DTT) modes. The outage performance of the FD CNOMA system with both SIC and imperfect SIC was derived. In [16], the performance of the EH scheme for a TWRN was investigated showing that the hybrid-decode-amplify-and-forward (HDAF) protocol outperforms both two conventional DF and AF protocols. Further, with the diversity technique at the receivers, the system outage probability of the proposed system can be reduced significantly to satisfy the requirements of some practical applications.

In [20], a PS approach-based SWIPT with a DF scheme was employed at the two-way relay to harvest energy from RF signals. SWIPT for the AF-based TWRNs was adopted in [21–23]. In [24], the authors investigated the resource allocation problem employing a robust multiuser wireless-powered full-duplex communication system, where the full-duplex information transmitter, powered by the multi-antenna energy transmitter, intends to send a confidential message to the information receiver. In this paper, we employ and compare two energy harvesting protocols, three-phase-PSR-based relay and five-phase-TSR-based relay, SWIPT with the DF scheme used at the two-way relay.

1.2. Motivation and Contribution. Motivated by spectrum efficiency and energy efficiency and user fairness issues, this paper develops two power-splitting relaying (PSR) and time-switching relaying (TSR) protocols SWIPT-based cooperative NOMA in DF-based TWRNs. Closed-form expressions of the performance metric in terms of OP and system throughput are derived. The main contributions of the paper are outlined as follows:

(i) A SWIPT-based CR-NOMA is developed for a TWRN consisting of two users and a relay node employing PSR and TSR EH protocols in DLT mode

(ii) Exact expressions of outage probability (OP) and system throughput (ST) are derived for both PSR and TSR protocols in the TWRN

(iii) The impacts of signal quality (i.e., transmitting signal-to-noise ratio (SNR)), EH coefficients, distance between users and relay node, and target data rate on the OP and ST are evaluated to identify their appropriateness in practical system models such as within buildings, urban, suburban, and rural

(iv) Numerical results are presented to verify the analytically derived expressions of OP and ST of both PSR and TSR protocols in CR-NOMA-based TWRNs. It is shown that the TSR protocol is superior to PSR achieving either a lower OP or a higher ST. It is further observed that the OP of both protocols suffers from significant changes according to the variation of the SNR and EH capability at the relay, distance between the nodes, and also the target rate

1.3. Organization. We structure the rest of the paper as follows. Section 2 presents the overall system model of the proposed two-way relay channel in a CR-NOMA system and assumptions. Section 3 describes in detail the performance analysis of both PSR and TSR protocols. Section 4 shows the simulation results. Finally, Section 5 concludes this paper and summarizes the key findings.

Notations. In this paper, $E[\cdot]$ represents expectation operation. $f_Y(x)(\cdot)$ and $F_Y(x)(\cdot)$ represent the probability density function (PDF) and the cumulative distribution function (CDF) of a random variable $Y \in \{h_i, g_i\}(\mathrm{x})$, respectively. $|h_i|^2$ and $|g_i|^2$ denote channel gains. $\beta_i (i \in 1, 2)$, $0 \le \beta_i \le 1$, denote the power splitting ratio at D_1 and D_2, respectively. Assuming $\beta_1 \ge \beta_2$.

2. System Model

The operation principle of the TWRN model can be described as follows. Firstly, we assume that there is no direct link between users D_1 and D_2 due to physical obstacles and D_1 is farther from R than D_2. Secondly, the users D_1 and D_2 exchange their information via the relay R's assistance. Specifically, D_1 and D_2 transmit their signals x_1 and x_2 with the transmit power P_{D_1} and P_{D_2} to R, respectively, and R harvests the energy from D_1 and D_2. R then transmits the superimposed NOMA signal with the power P_r^X, $X \in \{\mathrm{PSR}, \mathrm{TSR}\}$, which is combined by x_1 and x_2, to D_1 and D_2. Lastly, each pair of separate transmitting/receiving antennas is equipped for each user and the relay to ensure two-way transmission. Specifically, we use one transmitting antenna and one receiving antenna at each user as well as at the relay. All wireless links are assumed to experience Rayleigh fading along with Additive White Gaussian Noise (AWGN) having zero mean and variance N_0. As shown in Figure 1, h_1, g_1, h_2, and g_2

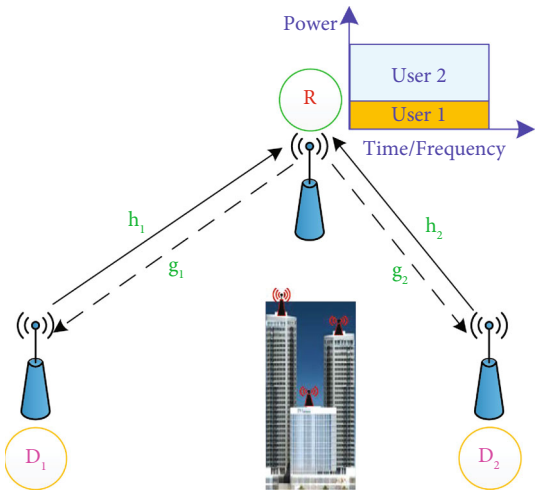

Figure 1: System model.

are the channel power gains of the links $D_1 \longrightarrow R$, $R \longrightarrow D_1$, $D_2 \longrightarrow R$, and $R \longrightarrow D_2$, respectively, each of which has an average channel gain of Ω_i, $i \in \{1, 2\}$. x_1 and x_2 denote the transmitted signals from D_1 and D_2. It is assumed that all nodes in the system model are accountable for applying the proposed design in this paper based on the available channel state information related to all wireless links. Without loss of generality, it is assumed that the fading gains in all related links are the Rayleigh distribution, and their probability density function (PDF) of exponentially random variables is given by

$$\begin{aligned} f_{|h_i|^2}(x) &= \frac{1}{\Omega_{h_i}} e^{-x/\Omega_{h_i}}, \quad i \in \{1, 2\}, \\ f_{|g_i|^2}(x) &= \frac{1}{\Omega_{g_i}} e^{-x/\Omega_{g_i}}, \quad i \in \{1, 2\}. \end{aligned} \tag{1}$$

The cumulative distribution function (CDF) of exponentially random variables is given by

$$\begin{aligned} F_{|h_i|^2}(x) &= 1 - e^{-x/\Omega_{h_i}}, \quad i \in \{1, 2\}, \\ F_{|g_i|^2}(x) &= 1 - e^{-x/\Omega_{g_i}}, \quad i \in \{1, 2\}. \end{aligned} \tag{2}$$

2.1. Energy Harvesting at R. At R, two energy harvesting protocols including three-phase-PSR-based R and five-phase-TSR-based R are sequentially considered.

2.1.1. Energy Harvesting at Three-Phase-PSR-Based R. Figure 2 illustrates the communication block diagram of the three-phase-PSR-based R protocol for EH and IP at the relay. P_{D_1} and P_{D_2} are the power of the received signal $y_r(t)$ at the relay, and T is the total transmitting time.

T is divided into three different time slots. In the first time slot α_1, the relay harvests the energy E_1 and the transmitted signal x_1 from D_1 and decodes x_1. In the second time slot α_2, the relay harvests the energy E_2 and the signal x_2 from D_2 and decodes x_2. Finally, the remaining time slot $(1 - \alpha_1 - \alpha_2)$, the relay forwards the signals to two users D_1 and D_2, $\alpha_i (i \in 1, 2)$, $0 \le \alpha_i \le 1$, and assuming $\alpha_1 \ge \alpha_2$.

In the first time slot and the second time slot of T, the power of the received signals, i.e., $\beta_1 P_{D_1}$ and $\beta_2 P_{D_2}$, are used for the EH, and the remaining power, i.e., $(1 - \beta_1)P_{D_1}$ and $(1 - \beta_2)P_{D_2}$, are used for the IP at D_1 and D_2, respectively. We denote x_1 and x_2 as the normalized transmitted signals by D_1 and D_2 with unity power, i.e., $E[x_1^2] = E[x_2^2] = 1$. The total transmission process is divided into a series of time slots. During the nth time slot, D_1 and D_2 transmit $x_1(t)$ and $x_2(t)$ with the power of P_{D_1} and P_{D_2}, respectively, while the relay transmits the superimposed NOMA signal $x_r(t)$ with the power of P_r^X. Thus, the transmitted signal expression at $D_i (i \in 1, 2)$ is given by

$$D_1(t) = \left(\sqrt{P_{D_1}} x_1(t)\right), \tag{3}$$

$$D_2(t) = \left(\sqrt{P_{D_2}} x_2(t)\right), \tag{4}$$

where a_1 and a_2 denote the power allocation coefficients for data symbol x_1 and x_2, respectively. The observed signal at R can be given by

$$\begin{aligned} y_{R,D_1}(t) &= h_1 D_1(t) + n_{R_1}(t) = h_1\left(\sqrt{P_{D_1}} x_1(t)\right) + n_{R_1}(t), \\ y_{R,D_2}(t) &= h_2 D_2(t) + n_{R_2}(t) = h_2\left(\sqrt{P_{D_2}} x_2(t)\right) + n_{R_2}(t), \\ y_R(t) &= y_{R,D_1}(t) + y_{R,D_2}(t) \\ &= h_1\left(\sqrt{P_{D_1}} x_1(t)\right) + h_2\left(\sqrt{P_{D_2}} x_2(t)\right) + n_R(t), \end{aligned} \tag{5}$$

where assuming $n_R(t) = n_{R_1}(t) + n_{R_2}(t)$ is AWGN with zero mean and variance N_0 at R.

The harvested energy is consumed by the relay for forwarding the information from the relay to the user. With a given $\beta_i (i \in 1, 2)$, it can affect the throughput of the users. The following sections analyze the EH and the IP at the PSR protocol exploiting the relay.

The power splitter divides the received signal $y_r(t)$ into $\beta_i : 1 - \beta_i$ ratio in which $\sqrt{\beta_i} y_r(t)$ is used for the EH and $\sqrt{1 - \beta_i} y_r(t)$ is used for the IP.

The received power at R to harvest the energy is given as

$$\begin{aligned} y_{\mathrm{EH},R}(t) &= \sqrt{\beta_i} y_R(t) = \sqrt{\beta_1} h_1\left(\sqrt{P_{D_1}} x_1(t)\right) \\ &\quad + \sqrt{\beta_2} h_2\left(\sqrt{P_{D_2}} x_2(t)\right) + \left(\sqrt{\beta_1} + \sqrt{\beta_2}\right) n_R(t). \end{aligned} \tag{6}$$

The harvested energy $E_{D_1}^{\mathrm{PSR}}$ at R due to the user D_1 is given by

$$E_{D_1}^{\mathrm{PSR}} = \eta \beta_1 P_{D_1} |h_1|^2 \alpha_1. \tag{7}$$

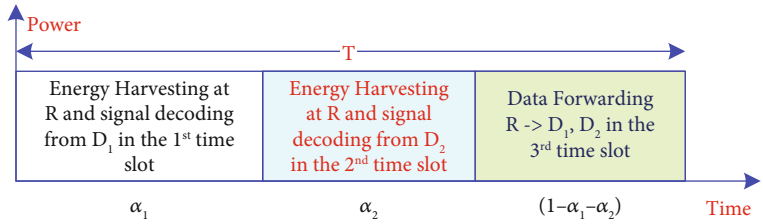

Figure 2: The PSR-based R protocol of EH and IP.

The harvested energy $E_{D_2}^{\mathrm{PSR}}$ at R due to the user D_2 is given by

$$E_{D_2}^{\mathrm{PSR}} = \eta\beta_2 P_{D_1}|h_2|^2\alpha_2. \tag{8}$$

Assuming $P_{D_1} = P_{D_2} = P$, the total harvested energy at the relay is given by

$$\begin{aligned} E_{\mathrm{tot}}^{\mathrm{PSR}} &= \sum_{i=1}^{2} E_{D_i}^{\mathrm{PSR}} \\ &= E_{D_1}^{\mathrm{PSR}} + E_{D_2}^{\mathrm{PSR}} \\ &= \eta\beta_1 P_{D_1}|h_1|^2\alpha_1 + \eta\beta_2 P_{D_2}|h_2|^2\alpha_2 \\ &= \eta P\left(\beta_1|h_1|^2\alpha_1 + \beta_2|h_2|^2\alpha_2\right), \end{aligned} \tag{9}$$

where $E_{\mathrm{tot}}^{\mathrm{PSR}}$ is the total harvested energy at the relay and $0 < \eta < 1$ is the energy conversion efficiency. η depends on the EH circuitry.

The harvested power at the relay is given by

$$P_r^{\mathrm{PSR}} = \frac{E_{\mathrm{tot}}^{\mathrm{PSR}}}{(\alpha_1 + \alpha_2)} = \frac{\eta P\left(\beta_1|h_1|^2\alpha_1 + \beta_2|h_2|^2\alpha_2\right)}{\alpha_1 + \alpha_2}. \tag{10}$$

2.1.2. Energy Harvesting at Five-Phase-TSR-Based R. Similar to three-phase-PSR-based R, the communication block diagram of the TSR-based R protocol for EH and IP at the relay is plotted in Figure 3. T denotes the total transmitting time block. As shown in Figure 3, R harvests the energy from D_1 in the first time slot $\alpha T/2$, R harvests the energy from D_2 in the second time slot $\alpha T/2$, D_1 transmits the information to R in the third time slot $(1-\alpha)T/3$, D_2 transmits the information to R in the fourth time slot $(1-\alpha)T/3$, and R transmits the signals to D_i $(i = 1, 2)$ in the remaining time slot $(1-\alpha)T/3$.

The harvested energy at R due to D_1 is given by

$$E_{D_1}^{\mathrm{TSR}} = \eta P_{D_1}|h_1|^2\left(\frac{\alpha T}{2}\right). \tag{11}$$

The harvested energy at R due to D_2 is given by

$$E_{D_2}^{\mathrm{TSR}} = \eta P_{D_2}|h_2|^2\left(\frac{\alpha T}{2}\right). \tag{12}$$

The total harvested energy at the relay is given by

$$E_{\mathrm{tot}}^{\mathrm{TSR}} = \sum_{i=1}^{2} E_{D_i}^{\mathrm{TSR}} = E_{D_1}^{\mathrm{TSR}} + E_{D_2}^{\mathrm{TSR}} = \eta\alpha P\left(|h_1|^2 + |h_2|^2\right)\left(\frac{T}{2}\right), \tag{13}$$

where α, $0 < \alpha < 1$, is the fraction of the time block in which relay harvests energy from the source signal.

The normalized transmit power at R is obtained from the harvested energy $E_{\mathrm{tot}}^{\mathrm{TSR}}$ over the time $(1-\alpha)T/3$ to forward the decoded signals to D_i $(i = 1, 2)$:

$$P_r^{\mathrm{TSR}} = \frac{E_{\mathrm{tot}}^{\mathrm{TSR}}}{(1-\alpha/3)T} = \frac{3E_{\mathrm{tot}}^{\mathrm{TSR}}}{(1-\alpha)T} = \frac{3}{2(1-\alpha)}\eta\alpha P\left(|h_1|^2 + |h_2|^2\right). \tag{14}$$

2.2. Information Processing

2.2.1. Information Processing at Three-Phase-PSR-Based R. The received signal at R for PSR protocol to process information is given by

$$\begin{aligned} y_{\mathrm{IP},R}^{\mathrm{PSR}}(t) &= \sqrt{(1-\beta_i)}\,y_R(t) = \sqrt{(1-\beta_1)P_{D_1}}\,h_1x_1(t) \\ &\quad + \sqrt{(1-\beta_2)P_{D_2}}\,h_2x_2(t) \\ &\quad + \left(\sqrt{(1-\beta_1)} + \sqrt{(1-\beta_2)}\right)n_R(t). \end{aligned} \tag{15}$$

The data $y_{\mathrm{IP},R}^{\mathrm{PSR}}(t)$ is converted to a sampled baseband data $y_{\mathrm{IP},R}^{\mathrm{PSR}}(k)$ by the RFBCU at R. Similar to [25] (Eq. (20)), $y_{\mathrm{IP},R}^{\mathrm{PSR}}(k)$ can be expressed as

$$\begin{aligned} y_{\mathrm{IP},R}^{\mathrm{PSR}}(k) &= \sqrt{(1-\beta_i)}\,y_R(k) = \sqrt{(1-\beta_1)P}\,h_1x_1(k) \\ &\quad + \sqrt{(1-\beta_2)P}\,h_2x_2(k) \\ &\quad + \left(\sqrt{(1-\beta_1)} + \sqrt{(1-\beta_2)}\right)n_R(t) + n_R^c(k), \end{aligned} \tag{16}$$

where $n_R^c(k)$ is AWGN at the RFBCU of R.

2.2.2. Information Processing at Five-Phase-TSR-Based R. To decode the data of D_1 and D_2, the RFBCU at R converts the received RF data $y_R(t)$ in Equation (3) into a sampled baseband data $y_{\mathrm{IP},R}^{\mathrm{PSR}}(k)$ in the first interval time $(1-\alpha)T/2$. The

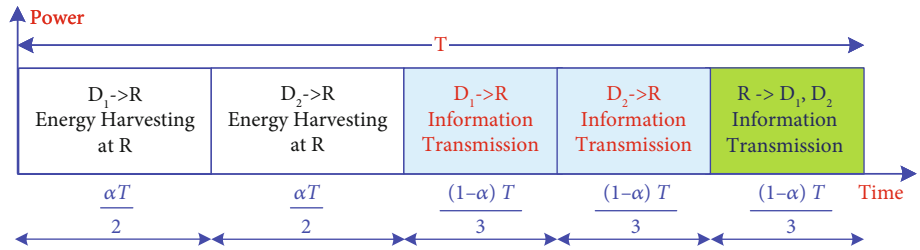

Figure 3: The TSR-based R protocol of EH and IP.

sampled signal $y_{\mathrm{IP},R}^{\mathrm{PSR}}(k)$ is explicitly expressed as follows [25] (Eq. (3)):

$$y_{\mathrm{IP},R}^{\mathrm{TSR}}(k) = Ph_1x_1(k) + Ph_2x_2(k) + n_R(k) + n_R^c(k). \tag{17}$$

Based on the NOMA principle as well as perfect SIC, the relay first decodes the signal x_1 which is transmitted by the user with more allocated power. The signal-to-interference plus noise ratio (SINR) at the relay is given by

$$\gamma_{1,R} = \frac{\psi_{I_1}\rho|h_1|^2}{\psi_{I_2}\rho|h_2|^2 + 1}, \tag{18}$$

where $\rho = P/N_0$ is the signal-to-noise ratio (SNR).

After decoding and cancelling x_1 from the received signals, the relay decodes x_2, and its SINR is given by

$$\gamma_{2,R} = \psi_{I_2}\rho|h_2|^2, \tag{19}$$

where $\psi_{I_i}(i \in 1, 2)$ is the IP coefficient of the PSR and TSR at the relay and is given by

$$\begin{cases} \psi_{I_1} = \dfrac{1-\beta_1}{3-\beta_1-\beta_2+2\sqrt{(1-\beta_1)(1-\beta_2)}}, \psi_{I_2} = \dfrac{1-\beta_2}{3-\beta_1-\beta_2+2\sqrt{(1-\beta_1)(1-\beta_2)}}, & \text{for PSR,} \\ \psi_{I_1} = \psi_{I_2} = \dfrac{1}{2}, & \text{for TSR.} \end{cases} \tag{20}$$

2.2.3. Information Processing at the Users $D_i(i \in 1, 2)$. According to the NOMA principle, the relay forwards the superposition coding signal, i.e., $\sqrt{P_r^X}(\sqrt{a_1}x_1 + \sqrt{a_2}x_2)$ $(X \in \mathrm{PSR}, \mathrm{TSR})$, to two users D_1 and D_1. Hence, the received signal at $D_i(i \in 1, 2)$ is expressed by

$$y_{D_i} = g_i\left(\sqrt{a_1P_r^X}x_1 + \sqrt{a_2P_r^X}x_2\right) + n_{D_i}, \tag{21}$$

where $g_i(g \in \{1, 2\})$ is the Rayleigh channel from the relay to D_i. a_1 and a_2 are power allocation coefficients of x_1 and x_2, respectively. n_{D_i} is the AWGN with zero mean and variance N_0 at D_i.

Following the NOMA principle, x_1, namely, the desired signal of D_2, is allocated more power than x_2 to ensure fairness between D_1 and D_2. Therefore, $a_1 > a_2$ and $a_1 + a_2 = 1$.

The signals $y_{D_i}(i \in 1, 2)$ are received by D_1 and D_2. The strength of the signal x_1 is higher than that of signal x_2 due to $a_1 > a_2$. The signal x_1 is detected by D_2, and its SINR is given by

$$\gamma_{1,D_2} = \frac{a_1P_r^X|g_2|^2}{a_2P_r^X|g_2|^2 + N_0} = \frac{a_1|g_2|^2\psi_E\rho\left(|h_1|^2 + |h_2|^2\right)}{a_2|g_2|^2\psi_E\rho\left(|h_1|^2 + |h_2|^2\right) + 1}, \tag{22}$$

where ψ_E is the EH coefficient of PSR and TSR at the relay and is given by

$$\psi_E = \begin{cases} \beta\eta, & \text{for PSR,} \\ \dfrac{3\alpha\eta}{2(1-\alpha)}, & \text{for TSR.} \end{cases} \tag{23}$$

The SINR to detect x_1 at D_1 is given by

$$\gamma_{1,D_1} = \frac{a_1P_r|g_1|^2}{a_2P_r|g_1|^2 + N_0} = \frac{a_1|g_1|^2\psi_E\rho\left(|h_1|^2 + |h_2|^2\right)}{a_2|g_1|^2\psi_E\rho\left(|h_1|^2 + |h_2|^2\right) + 1}. \tag{24}$$

Table 1: Definition of system parameters.

Parameters	Notations	Values
The power allocation coefficients	$\{a_1, a_2\}$	{0.8,0.2}
The power allocation ratios	$\{\beta_1, \beta_2\}$	{0.2,0.2}
The time slots	$\{\alpha_1, \alpha_2\}$	{1/3, 1/3}
The total transmitting time	T	1
The path-loss exponent	m	3
The normalized distance between D_1 and R	d	0.3
The target rates of two links (Link1, Link2)	$\{R_1, R_2\}$	{3(BPCU), 1(BPCU)}
The energy conversion efficiency coefficient	η	{0.8}
The channel gains	$\{\Omega_{h_1}, \Omega_{g_1}, \Omega_{h_2}, \Omega_{g_2}\}$	$\{d^{-m}, d^{-m}\}, \{(1-d)^{-m}, (1-d)^{-m}\}$

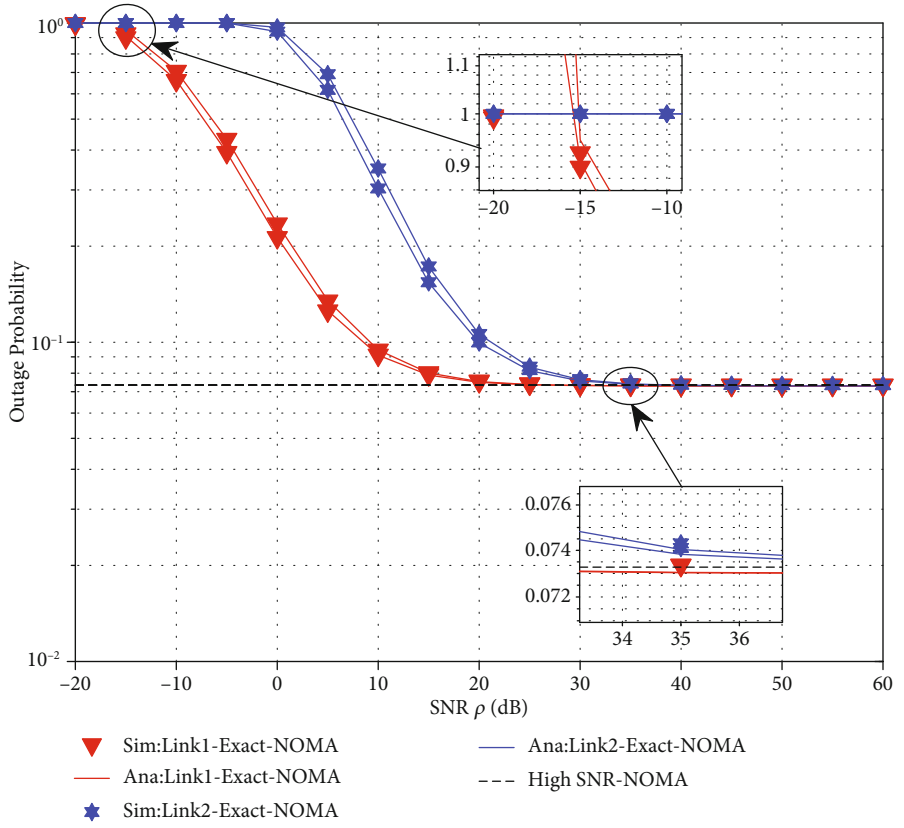

Figure 4: OP versus transmitting SNR for PSR (blue line) and TSR (red line) protocols.

After SIC x_1 at D_1, x_2 is decoded by D_1, and its SINR is given by

$$\gamma_{2,D_1} = a_2 P_r^X |g_1|^2 = a_2 |g_1|^2 \psi_E \rho \left(|h_1|^2 + |h_2|^2\right). \quad (25)$$

3. Performance Analysis

3.1. Outage Performance

3.1.1. The OP of the Link $D_1 \longrightarrow R \longrightarrow D_2$ (Link1). Based on NOMA, the OP of Link1 is described as follows. The relay detects the signal x_1, then D_2 also detects the signal x_1. Therefore, the OP of Link1 is given by

$$P_{D_2,X} = 1 - \Pr\left(\gamma_{1,R} > \gamma_{\text{th}_2}, \gamma_{1,D_2} > \gamma_{\text{th}_2}\right), \quad (26)$$

where $\gamma_{\text{th}_2} = 2^{R_2} - 1$ is the threshold SINR in which R_2 is the target rate of this link. The following finding of the OP of Link1 is given by Theorem 1.

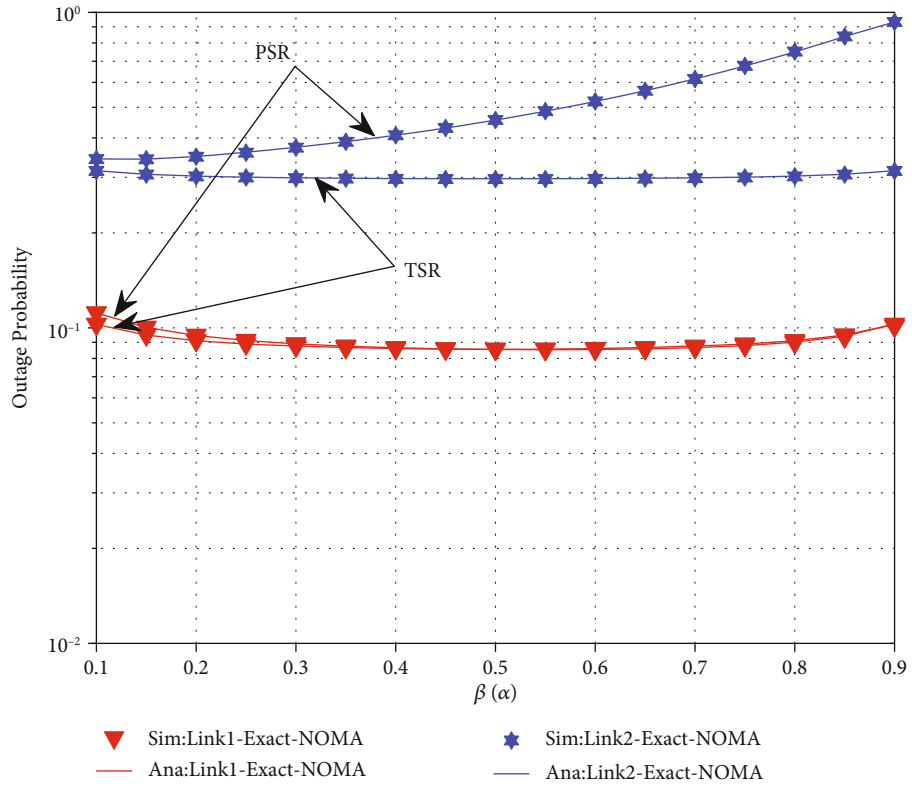

Figure 5: OP versus the transmitting EH coefficients for PSR and TSR protocols.

Theorem 1. *The OP of Link1 is given by*

$$P_{D_2,X} = 1 - \left\{ \frac{2e^{-\Phi/\Omega_{h_1}+\phi\delta}}{\Omega_{g_2}\Omega_{h_2}\phi} \sqrt{\phi\varphi\Omega_{g_2}} K_1\left(2\sqrt{\frac{\phi\varphi}{\Omega_{g_2}}}\right) + \frac{1}{\Omega_{g_2}\Omega_{h_2}\xi}\left[2\sqrt{\frac{\Theta\Omega_{g_2}}{\Omega_{h_1}}} K_1\left(2\sqrt{\frac{\Theta}{\Omega_{h_1}\Omega_{g_2}}}\right) - e^{\xi\delta} 2\sqrt{\zeta\Omega_{g_2}} K_1\left(2\sqrt{\frac{\zeta}{\Omega_{g_2}}}\right)\right]\right\}. \tag{27}$$

Proof. See Appendix A. □

3.1.2. The OP of the Link $D_2 \longrightarrow R \longrightarrow D_1$ (Link2). Similarly, the OP of Link2 is described as follows. The relay detects the signal x_1 and then detects the signal x_2, and then, D_1 also detects the signal x_1 and wishes to successfully detect the signal x_2.

Therefore, the OP of Link2 is given by

$$P_{D_1,X} = 1 - \Pr\left(\gamma_{1,R} > \gamma_{\text{th}_2}, \gamma_{2,R} > \gamma_{\gamma_{\text{th}_1}}, \gamma_{1,D_1} > \gamma_{\text{th}_2}, \gamma_{2,D_1} > \gamma_{\gamma_{\text{th}_1}}\right), \tag{28}$$

where $\gamma_{\text{th}_1} = 2^{R_1} - 1$ is the threshold SINR in which R_1 is the target rate of Link2. The following finding of the OP of Link2 is given by Theorem 2.

Theorem 2. *The OP of Link2 is given by*

$$P_{D_1,X} = 1 - \left[\frac{e^{-\Phi/\Omega_{h_1}+\delta\phi}}{\Omega_{h_2}\phi}\gamma\left(1, \frac{\bar{\omega}}{\Omega_{g_1}(\bar{\Phi}+\delta)}, \frac{\phi\bar{\omega}}{\Omega_{g_1}}\right) + \frac{e^{-\Phi/\Omega_{h_1}-\bar{\omega}/\Omega_{g_1}(\bar{\Phi}+\delta)-\bar{\Phi}\phi}}{\Omega_{h_2}\phi} + \frac{1}{\Omega_{h_2}\Omega_{g_1}}\int_{\bar{\Phi}}^{\infty} e^{-x\xi}\int_0^{\bar{\omega}/x+\delta} e^{-y/\Omega_{g_1}-\ell/y\Omega_{h_1}}\,dxdy\right]. \tag{29}$$

Proof. See Appendix B. □

3.2. The System Throughput. In this system model, Link1 and Link2 simultaneously transmit signals x_1 and x_2 at a constant rate of R_1 and R_2, respectively. Therefore, the system throughput depends only on the OP caused by the wireless fading channels, which is calculated by

$$\tau_X = \left(1 - P_{D_1,X}\right)R_1 + \left(1 - P_{D_2,X}\right)R_2. \tag{30}$$

4. Simulation Results

In this section, several numerical results are provided to verify the analytical results which were discussed in the aforementioned sections. In particular, the main parameters of the system model can be seen in Table 1.

Figure 4 describes the OP of Link1 and Link2 versus SNR. The SNR is set from -20 to 60 dB. It is seen that the

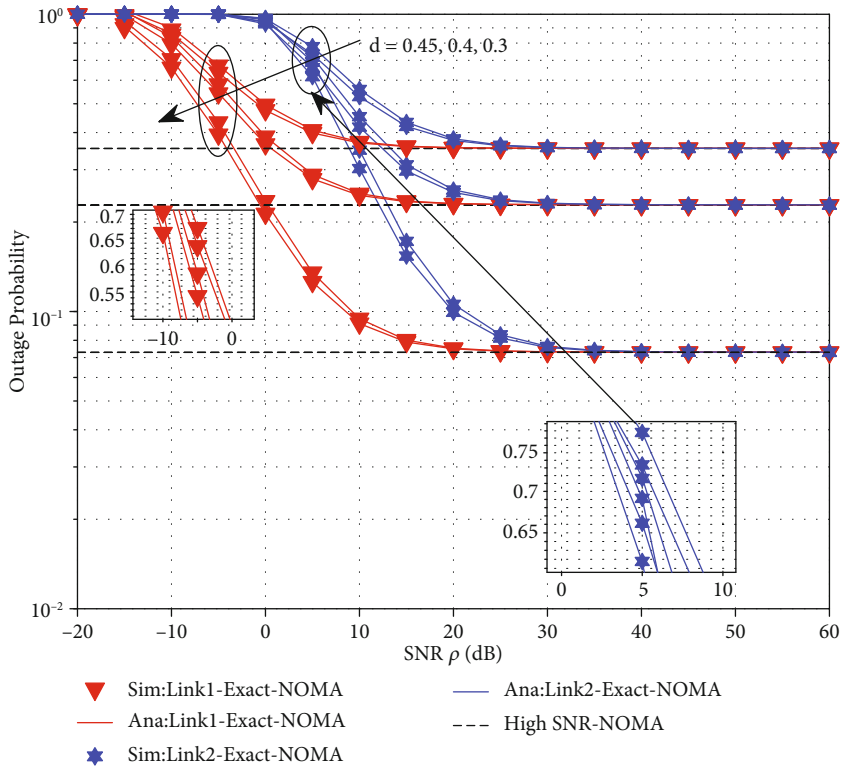

Figure 6: OP versus SNR and different values of d (PSR (blue line) and TSR (red line)).

OP of both links for TSR is always lower than that for PSR. Specifically, in SNR range of from -20 to -15 dB, both links have the OP of 10^0 which results in the outage for these both links. In SNR range of from -15 to 5 dB, while Link1 is still in the outage, the OP of Link1 decreases quickly. In SNR range of from 5 to 35 dB, the OP of Link2 starts decreasing strongly while that of Link1 reduces gradually and is asymptotic to the high SNR curve (i.e., about 1.2×10^{-1}). In SNR range of from 35 to 40 dB, the OP of Link1 still keeps constant and the OP of Link2 decreases gradually and then is asymptotic to the high SNR curve. In the remaining SNR, the OP of both users is constant and overlaps the high SNR curve. It is observed that the slope of the curves of Link1 is earlier than that of Link2. In addition, in the comparison between the two links, the OP of Link1 is always lower than that of Link2. These can be explained based on Equations (25) and (27).

Similarly, Figure 5 plots the OP of two links versus power splitting ratio β for PSR protocol and time switching fraction α for TSR protocol with the assumption that $\alpha = \beta$. The OP of Link1 for both protocols PSR and TSR is always lower than that of Link2. The gap of the OP between these two links is about 60%. In particular, the OP of Link1 for PSR is always higher than that for TSR. However, this OP of Link2 for both PSR and TSR has a change in different β ranges. Specifically, in β range of from 0.1 to around 0.32, the OP of Link2 for TSR is lower than that for PSR while this OP for TSR is higher than that for PSR in the remaining β range. An observation from the figure shows that the curves of the OP have a small change during the β axis. They considerably vary in β range of from 0.1 to 0.2 and from 0.8 to 0.9. It implies that when β is chosen in a range of 0.2 to 0.8, the OP of the system is almost kept constant. It is because Equations (25) and (27) contain the terms ψ_I, ψ_E which directly depend on variables of β and α.

The dependence of the OP on SNR and distance between the nodes is shown in Figure 6. When the distance d increases, the OP for both chain links are also increased. Similar to Figure 4, it is seen that the shape of the OP curves seems to be uniform. This means that the OP of both links decreases quickly in a certain SNR range and then keeps constant in the remaining SNR range. It is noted that when SNR tends towards higher value (about from 20 to 60 dB), the OP is asymptotical to high SNR curves and then overlaps each other. The larger the distance d, the higher the outage probability and the more quickly the asymptote to high SNR curves.

Figure 7 shows the change of the OP according to different values of target rate R and SNR. When the SNR range is from -20 to 30 dB, the OP of both links decreases very quickly and its slopes are very high. The higher the target rate, the lower the OP. Link1 has a low OP as compared to Link2 in the SNR range of from -20 to 30 dB. The OP for this link changes more quickly than that for Link2. However, in the SNR range of from 30 to 60 dB, these outage probabilities tend to constant curves in which their values are equal to that of high SNR curves. In most cases, the PSR always achieves a higher OP as compared to TSR.

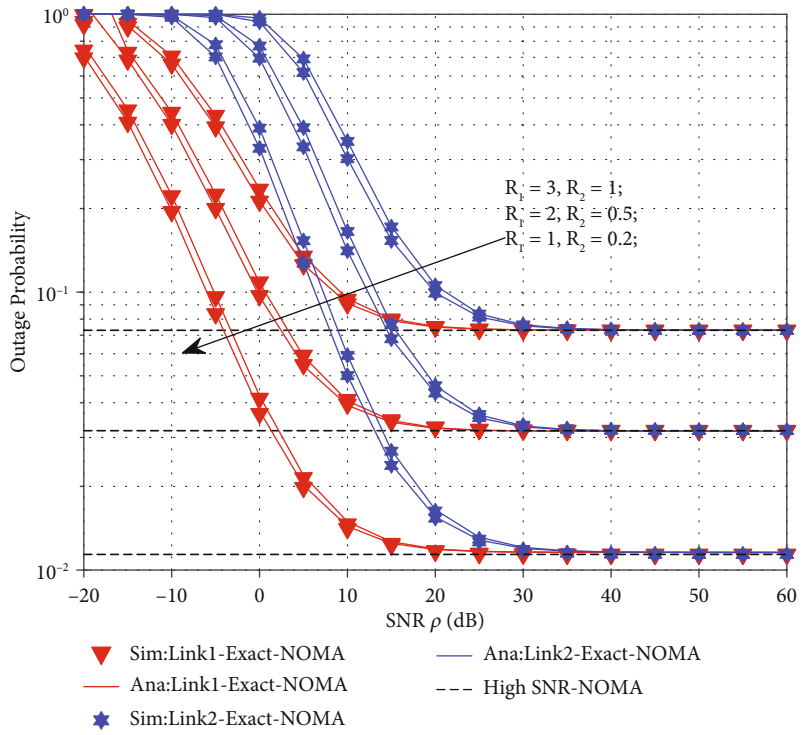

Figure 7: OP versus SNR and different values of R (PSR (blue line) and TSR (red line)).

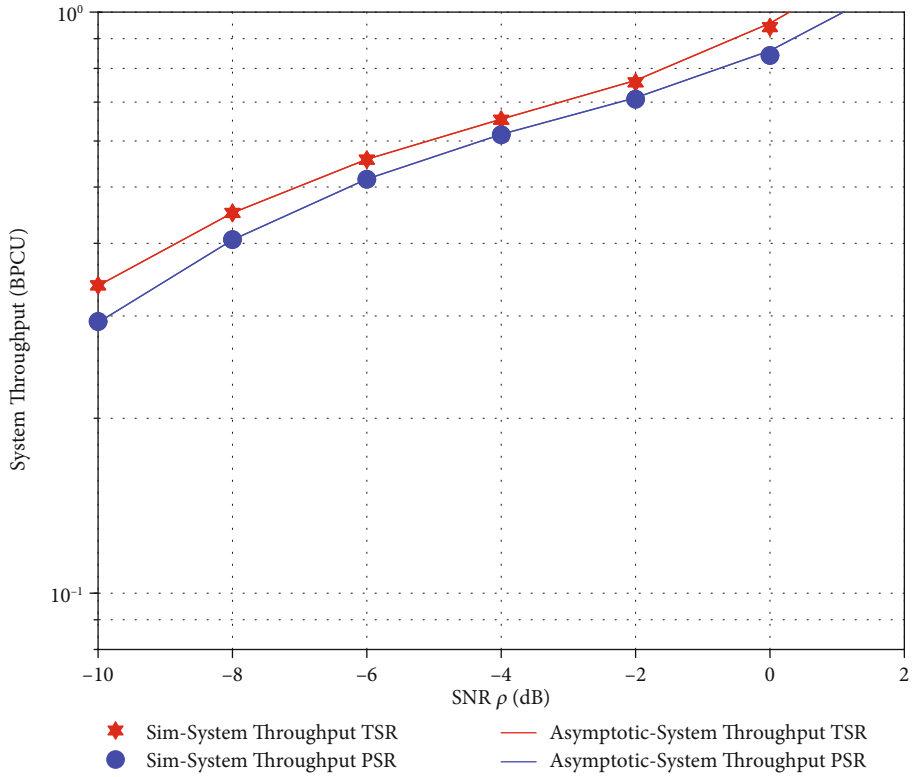

Figure 8: The system throughput versus SNR for PSR (blue line) and TSR (red line) protocols.

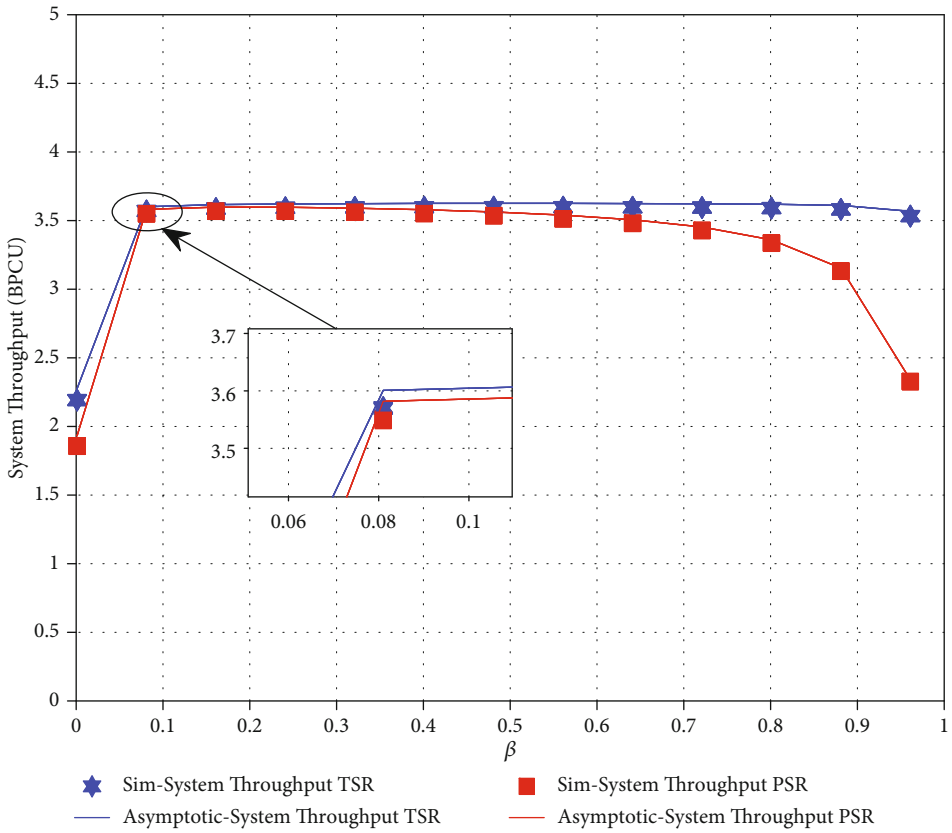

Figure 9: The system throughput versus the transmitting EH coefficients for PSR (blue line) and TSR (red line) protocols.

Figure 8 plots the system throughput for two protocols versus SNR. The SNR is set from -10 to 2 dB. It is observed that the system throughput increases with an increasing SNR. The PSR always obtains a lower throughput over the TSR in the overall scale of SNR. However, the gap between the two curves is almost constant and small. The ratio of the throughput between PSR and TSR is about 8%. To explain this difference, it is based on Equations (25) and (27). Furthermore, the increase of the system throughput according to SNR can be demonstrated by Equations (25) and (27).

Figure 9 shows the dependence of the system throughput for TPS and PSR versus energy harvesting coefficients. The system throughput for both protocols increases linearly in the β range of from 0 to 0.1. In the remaining β range, the system throughput for TSR is almost constant while that for PSR tends to decrease. In particular, the system throughput for PSR decreases strongly in the β range of from 0.7 to 1. This implies that the system throughput for TSR is not affected by the energy harvesting coefficients in most cases while that for PSR considerably suffers from the impacts of these coefficients. It can be explained based on Equations (21) and (28). Furthermore, the TSR always achieves a high throughput than PSR.

5. Conclusion

Two three-phase-PSR-based D_1 and five-phase-TSR based D_1 protocols for EH and IP in a two-way relay CR-NOMA system have been presented in this paper. The closed-form expressions of OP and throughput for Link1 and Link2 were derived. The dependence of OP and throughput on SNR, energy harvesting coefficients, distance between the nodes, and target rate were also evaluated. The simulation results showed that the TSR achieved a lower OP and a higher system throughput over the TSR. The OP decreased significantly in the low SNR region and is asymptotic to the high SNR curve in the high SNR region. The system throughput was almost kept constant in the β range. Furthermore, the larger the distance and target rate, the worse the OP.

Appendix

A. Proof of Theorem 1

In this appendix, we present the proof of (27). Plugging (18) and (22) into (26), (26) is rewritten as follows:

$$\begin{aligned} P_{D_2} &= 1 - \Pr\left(\frac{\psi_I \rho |h_1|^2}{\psi_I \rho |h_2|^2 + 1} > \gamma_{\text{th}_2}, \frac{a_1 |g_2|^2 \psi_E \rho \left(|h_1|^2 + |h_2|^2\right)}{a_2 \theta |g_2|^2 \psi_E \rho \left(|h_1|^2 + |h_2|^2\right) + 1} > \gamma_{\text{th}_2}\right) \\ &= 1 - \Pr\left(|h_1|^2 > \frac{\gamma_{\text{th}_2}}{\rho \psi_I}\left(\psi_I \rho |h_2|^2 + 1\right), |g_2|^2 \left(|h_1|^2 + |h_2|^2\right) > \frac{\gamma_{\text{th}_2}}{\Phi(a_1 - \gamma_2 a_2)}\right) \\ &= 1 - \Pr\left(|h_1|^2 > \Phi\left(\psi_I \rho |h_2|^2 + 1\right), |h_1|^2 > \frac{\Theta}{|g_2|^2} - |h_2|^2\right), \end{aligned} \tag{A.1}$$

where $\Phi = \gamma_{th_2}/\rho\psi_I, \Theta = \gamma_{th_2}/\theta(a_1 - \gamma_2 a_2)$

$$P_{D_2} = 1 - \left[\underbrace{\Pr\left(|h_1|^2 > \Phi\left(\psi_I \rho |h_2|^2 + 1\right), |h_2|^2 > \frac{\Theta}{(\Phi\psi_I\rho + 1)|g_2|^2} - \frac{\Phi}{(\Phi\psi_I\rho + 1)} \right)}_{I_1} + \underbrace{\Pr\left(|h_1|^2 > \frac{\Theta}{|g_2|^2} - |h_2|^2, |h_2|^2 < \frac{\Theta}{(\Phi\psi_I\rho + 1)|g_2|^2} - \frac{\Phi}{(\Phi\psi_I\rho + 1)} \right)}_{I_2} \right], \tag{A.2}$$

where $\Pr(\cdot)$ denotes the probability function. We have the following formulas to use for the calculation. I_1 can be calculated as follows:

$$\begin{aligned} I_1 &= \Pr\left(|h_1|^2 > \Phi\left(\psi_I \rho |h_2|^2 + 1\right), |h_2|^2 > \frac{\Theta}{(\Phi\psi_I\rho + 1)|g_2|^2} - \frac{\Phi}{(\Phi\psi_I\rho + 1)} \right) \\ &= \Pr\left(|h_1|^2 > \Phi\left(\psi_I \rho |h_2|^2 + 1\right), |h_2|^2 > \frac{\varphi}{|g_2|^2} - \delta \right) \\ &= \int_0^\infty f_{|g_2|^2}(x) \int_{\varphi/x-\delta}^\infty f_{|h_2|^2}(y) \int_{\Phi(\psi_I\rho y+1)}^\infty f_{|h_1|^2}(z) dxdydz \\ &= \frac{1}{\Omega_{g_2}\Omega_{h_2}\Omega_{h_1}} \int_0^\infty e^{-x/\Omega_{g_2}} \int_{\varphi/x-\delta}^\infty e^{-y/\Omega_{h_2}} \int_{\Phi(\psi_I\rho y+1)}^\infty e^{-z/\Omega_{h_1}} dxdydz \\ &= \frac{e^{-\Phi/\Omega_{h_1}}}{\Omega_{g_2}\Omega_{h_2}} \int_0^\infty e^{-x/\Omega_{g_2}} \int_{\varphi/x-\delta}^\infty e^{-y\left(1/\Omega_{h_2} + \Phi\psi_I\rho/\Omega_{h_1}\right)} dxdy \\ &= \frac{e^{-\Phi/\Omega_{h_1}}}{\Omega_{g_2}\Omega_{h_2}} \int_0^\infty e^{-x/\Omega_{g_2}} \int_{\varphi/x-\delta}^\infty e^{-y\phi} dxdy = \frac{e^{-\Phi/\Omega_{h_1}+\phi\delta}}{\Omega_{g_2}\Omega_{h_2}\phi} \int_0^\infty e^{-\phi\varphi/x - x/\Omega_{g_2}} dx. \end{aligned} \tag{A.3}$$

Applying the formula $\int_0^\infty e^{-\beta/4x - \gamma x} dx = \sqrt{\beta/\gamma} K_1(\sqrt{\beta\gamma})$, where $K_1(\cdot)$ denotes the first-order modified Bessel function of the second kind [26] (Eq. (3.324.1)).

The expression I_1 is given by

$$\begin{aligned} I_1 &= \frac{e^{-\Phi/\Omega_{h_1}+\phi\delta}}{\Omega_{g_2}\Omega_{h_2}\phi} \int_0^\infty e^{-4\phi\varphi/4x - x/\Omega_{g_2}} dx \\ &= \frac{2e^{-\Phi/\Omega_{h_1}+\phi\delta}}{\Omega_{g_2}\Omega_{h_2}\phi} \sqrt{\phi\varphi\Omega_{g_2}} K_1\left(2\sqrt{\frac{\phi\varphi}{\Omega_{g_2}}}\right), \end{aligned} \tag{A.4}$$

where $\varphi = \Theta/(\Phi\psi_I\rho + 1), \delta = \Phi/(\Phi\psi_I\rho + 1), \phi = (1/\Omega_{h_2} + \Phi\psi_I\rho/\Omega_{h_1})$.

Similarly, I_2 can be computed as follows:

$$\begin{aligned} I_2 &= \Pr\left(|h_1|^2 > \Phi\left(\psi_I \rho |h_2|^2 + 1\right), |h_2|^2 < \frac{\Theta}{(\Phi\psi_I\rho + 1)|g_2|^2} - \frac{\Phi}{(\Phi\psi_I\rho + 1)} \right) \\ &= \Pr\left(|h_1|^2 > \Phi\left(\psi_I \rho |h_2|^2 + 1\right), |h_2|^2 < \frac{\varphi}{|g_2|^2} - \delta \right) \\ &= \int_0^\infty f_{|g_2|^2}(x) \int_0^{\varphi/x-\delta} f_{|h_2|^2}(y) \int_{\Theta/x-y}^\infty f_{|h_1|^2}(z) dxdydz \\ &= \frac{1}{\Omega_{g_2}\Omega_{h_2}\Omega_{h_1}} \int_0^\infty e^{-x/\Omega_{g_2}} \int_0^{\varphi/x-\delta} e^{-y/\Omega_{h_2}} \int_{\Theta/x-y}^\infty e^{-z/\Omega_{h_1}} dxdydz \\ &= \frac{1}{\Omega_{g_2}\Omega_{h_2}} \int_0^\infty e^{-x/\Omega_{g_2} - \Theta/\Omega_{h_1}x} \int_0^{\varphi/x-\delta} e^{-y\left(1/\Omega_{h_2} - 1/\Omega_{h_1}\right)} dxdy \\ &= \frac{1}{\Omega_{g_2}\Omega_{h_2}} \int_0^\infty e^{-x/\Omega_{g_2} - \Theta/\Omega_{h_1}x} \int_0^{\varphi/x-\delta} e^{-y\xi} dxdy \\ &= \frac{1}{\Omega_{g_2}\Omega_{h_2}\xi} \int_0^\infty e^{-x/\Omega_{g_2} - \Theta/\Omega_{h_1}x} \left(1 - e^{-(\varphi/x-\delta)\xi}\right) dx \\ &= \frac{1}{\Omega_{g_2}\Omega_{h_2}\xi} \left[\int_0^\infty e^{-\Theta/\Omega_{h_1}x - x/\Omega_{g_2}} dx - e^{\xi\delta} \int_0^\infty e^{-x/\Omega_{g_2} - 1/x\left(\Theta/\Omega_{h_1} + \xi\varphi\right)} dx \right] \\ &= \frac{1}{\Omega_{g_2}\Omega_{h_2}\xi} \left[2\sqrt{\frac{\Theta\Omega_{g_2}}{\Omega_{h_1}}} K_1\left(2\sqrt{\frac{\Theta}{\Omega_{h_1}\Omega_{g_2}}}\right) - e^{\xi\delta} 2\sqrt{\zeta\Omega_{g_2}} K_1\left(2\sqrt{\frac{\zeta}{\Omega_{g_2}}}\right) \right], \end{aligned} \tag{A.5}$$

where $\xi = (1/\Omega_{h_2} - 1/\Omega_{h_1}), \zeta = (\Theta/\Omega_{h_1} + \xi\varphi)$.

By replacing I_1 and I_2 into (A.2), the formula of (27) can be derived. The proof is completed.

B. Proof of Theorem 2

In this appendix, we present the proof of (29). Plugging (18), (19), (24), and (25) into (28), (28) is rewritten as follows:

$$
\begin{aligned}
P_{D_1} &= 1-\Pr\left(\frac{\psi_I\rho|h_1|^2}{\psi_I\rho|h_2|^2+1}>\gamma_{\mathrm{th}_2},\psi_I\rho|h_2|^2>\gamma_{\mathrm{th}_1},\frac{a_1|g_1|^2\psi_E\rho(|h_1|^2+|h_2|^2)}{a_2|g_1|^2\psi_E\rho(|h_1|^2+|h_2|^2)+1}>\gamma_{\mathrm{th}_2},a_2\psi_E\rho|g_1|^2(|h_1|^2+|h_2|^2)>\gamma_{\mathrm{th}_1}\right)\\
&= 1-\Pr\left(|h_1|^2>\Phi\left(\psi_I\rho|h_2|^2+1\right),|h_1|^2>\frac{\ell}{|g_1|^2}-|h_2|^2,|h_2|^2>\bar{\Phi}\right)\\
&= 1-\left[\Pr\left(|h_1|^2>\Phi\left(\psi_I\rho|h_2|^2+1\right),|h_2|^2>\frac{\omega}{|g_1|^2}-\delta,|h_2|^2>\bar{\Phi}\right)+\Pr\left(|h_1|^2>\frac{\ell}{|g_1|^2}-|h_2|^2,|h_2|^2<\frac{\omega}{|g_1|^2}-\delta,|h_2|^2>\bar{\Phi}\right)\right]\\
&= 1-\Bigg[\underbrace{\Pr\left(|h_1|^2>\Phi\left(\psi_I\rho|h_2|^2+1\right),|h_2|^2>\frac{\omega}{|g_1|^2}-\delta,|g_1|^2<\frac{\omega}{(\bar{\Phi}+\delta)}\right)}_{J_1}+\underbrace{\Pr\left(|h_1|^2>\Phi\left(\psi_I\rho|h_2|^2+1\right),|h_2|^2>\bar{\Phi},|g_1|^2>\frac{\omega}{(\bar{\Phi}+\delta)}\right)}_{J_2}+\underbrace{\Pr\left(|h_1|^2>\frac{\ell}{|g_1|^2}-|h_2|^2,|g_1|^2<\frac{\omega}{|h_2|^2+\delta},|h_2|^2>\bar{\Phi}\right)}_{J_3}\Bigg],
\end{aligned}
\tag{B.1}
$$

where $\Phi=\gamma_{\mathrm{th}_2}/\rho\psi_I$, $\bar{\Phi}=\gamma_{\mathrm{th}_1}/\rho\psi_I$, $\Theta=\gamma_{\mathrm{th}_2}/\psi_E\rho(a_1-\gamma_{\mathrm{th}_2}a_2)$, $\ell=\max(\Theta,\gamma_{\mathrm{th}_1}/a_2\psi_E\rho)$, $\omega=\ell/[\psi_I\rho\Phi+1]$, $\delta=\Phi/[\psi_I\rho\Phi+1]$.

Applying the PDF and CDF, J_1, J_2, and J_3 can be computed as follows:

$$
\begin{aligned}
J_1 &= \Pr\left(|h_1|^2>\Phi\left(\psi_I\rho|h_2|^2+1\right),|h_2|^2>\frac{\omega}{|g_1|^2}-\delta,|g_1|^2<\frac{\omega}{(\bar{\Phi}+\delta)}\right)\\
&= \int_0^{\omega/(\bar{\Phi}+\delta)} f_{|g_1|^2}(x)\int_{\omega/x-\delta}^{\infty} f_{|h_2|^2}(y)\left[1-F_{|h_1|^2}(\Phi(\psi_I\rho y+1))\right]dxdy\\
&= \frac{e^{-\Phi/\Omega_{h_1}}}{\Omega_{g_1}\Omega_{h_2}}\int_0^{\omega/(\bar{\Phi}+\delta)} e^{-x/\Omega_{g_1}}\int_{\omega/x-\delta}^{\infty} e^{-y\left(1/\Omega_{h_2}+\psi_I\rho\Phi/\Omega_{h_1}\right)}dxdy\\
&= \frac{e^{-\Phi/\Omega_{h_1}}}{\Omega_{g_1}\Omega_{h_2}}\int_0^{\omega/(\bar{\Phi}+\delta)} e^{-x/\Omega_{g_1}}\int_{\omega/x-\delta}^{\infty} e^{-y\phi}dxdy\\
&= \frac{e^{-\Phi/\Omega_{h_1}+\delta\phi}}{\Omega_{g_1}\Omega_{h_2}\phi}\int_0^{\omega/(\bar{\Phi}+\delta)} e^{-x/\Omega_{g_1}-\phi\omega/x}dx.
\end{aligned}
\tag{B.2}
$$

Applying $\int_0^x t^{\alpha-1}e^{-at-b/t}dt=a^{-\alpha}\gamma(\alpha,ax,ab)$, where $\gamma(.)$ represents the generalized incomplete gamma [25].

The expressions J_1 is given by

$$
J_1=\frac{e^{-\Phi/\Omega_{h_1}+\delta\phi}}{\Omega_{h_2}\phi}\gamma\left(1,\frac{\omega}{\Omega_{g_1}(\bar{\Phi}+\delta)},\frac{\phi\omega}{\Omega_{g_1}}\right),
\tag{B.3}
$$

where $\phi=(1/\Omega_{h_2}+\psi_I\rho\Phi/\Omega_{h_1})$.

The expressions J_2 is given by

$$
\begin{aligned}
J_2 &= \Pr\left(|h_1|^2>\Phi\left(\psi_I\rho|h_2|^2+1\right),|h_2|^2>\bar{\Phi},|g_1|^2>\frac{\omega}{(\bar{\Phi}+\delta)}\right)\\
&= \int_{\omega/(\bar{\Phi}+\delta)}^{\infty} f_{|g_1|^2}(x)\int_{\bar{\Phi}}^{\infty} f_{|h_2|^2}(y)\left[1-F_{|h_1|^2}(\Phi(\psi_I\rho y+1))\right]dxdy\\
&= \frac{e^{-\Phi/\Omega_{h_1}}}{\Omega_{g_1}\Omega_{h_2}}\int_{\omega/(\bar{\Phi}+\delta)}^{\infty} e^{-x/\Omega_{g_1}}\int_{\bar{\Phi}}^{\infty} e^{-y\phi}dxdy\\
&= \frac{e^{-\Phi/\Omega_{h_1}-\omega/\Omega_{g_1}(\bar{\Phi}+\delta)-\bar{\Phi}\phi}}{\Omega_{h_2}\phi}.
\end{aligned}
\tag{B.4}
$$

The expressions J_3 is given by

$$
\begin{aligned}
J_3 &= \Pr\left(|h_1|^2>\frac{\ell}{|g_1|^2}-|h_2|^2,|g_1|^2<\frac{\omega}{|h_2|^2+\delta},|h_2|^2>\bar{\Phi}\right)\\
&= \int_{\bar{\Phi}}^{\infty} f_{|h_2|^2}(x)\int_0^{\omega/x+\delta} f_{|g_1|^2}(y)\left[1-F_{|h_1|^2}\left(\frac{\ell}{y}-x\right)\right]dxdy\\
&= \frac{1}{\Omega_{h_2}\Omega_{g_1}}\int_{\bar{\Phi}}^{\infty} e^{-x/\Omega_{h_2}}\int_0^{\omega/x+\delta} e^{-y/\Omega_{g_1}}e^{-1/\Omega_{h_1}(\ell/y-x)}dxdy\\
&= \frac{1}{\Omega_{h_2}\Omega_{g_1}}\int_{\bar{\Phi}}^{\infty} e^{-x\xi}\int_0^{\omega/x+\delta} e^{-y/\Omega_{g_1}-\ell/y\Omega_{h_1}}dxdy,
\end{aligned}
\tag{B.5}
$$

where $\xi=1/\Omega_{h_2}-1/\Omega_{h_1}$. By replacing J_1, J_2, and J_3 into (B.1), the formula of (29) can be derived. The proof is completed.

Data Availability

The data used to support the findings of this study are included in the article.

Conflicts of Interest

The authors declare that there is no conflict of interest in this manuscript.

Authors' Contributions

Huu Q. Tran worked on conceptualization, methodology, software, formal analysis, and investigation. Huu Q. Tran worked on data curation and writing (original draft preparation). Huu Q. Tran and Quoc-Tuan Vien worked on validation and resources. Huu Q. Tran and Quoc-Tuan Vien worked on writing (reviewing and editing).

Acknowledgments

This study was self-funded by the authors.

References

[1] S. M. R. Islam, M. Zeng, and O. A. Dobre, "NOMA in 5G systems: exciting possibilities for enhancing spectral efficiency," 2017, https://arxiv.org/abs/1706.08215.

[2] Z. Ding, X. Lei, G. K. Karagiannidis, R. Schober, J. Yuan, and V. K. Bhargava, "A survey on non-orthogonal multiple access for 5G networks: research challenges and future trends," *IEEE Journal on Selected Areas in Communications*, vol. 35, no. 10, pp. 2181–2195, 2017.

[3] L. Dai, B. Wang, Z. Ding, Z. Wang, S. Chen, and L. Hanzo, "A survey of non-orthogonal multiple access for 5G," *IEEE communications surveys & tutorials*, vol. 20, no. 3, pp. 2294–2323, 2018.

[4] H. Q. Tran, T.-T. Nguyen, C. V. Phan, and Q.-T. Vien, "On the performance of NOMA in SWIPT systems with power-splitting relaying," in *2019 19th International Symposium on Communications and Information Technologies (ISCIT)*, pp. 255–259, Ho Chi Minh City, Vietnam, 2018.

[5] A. Benjebbovu, A. Li, Y. Saito, Y. Kishiyama, A. Harada, and T. Nakamura, "System-level performance of downlink NOMA for future LTE enhancements," in *2013 IEEE Globecom Workshops (GC Wkshps)*, vol. 20, pp. 66–70, Atlanta, GA, USA, 2013.

[6] A. Benjebbour, K. Saito, A. Li, Y. Kishiyama, and T. Nakamura, "Non-orthogonal multiple access (NOMA): concept, performance evaluation and experimental trials," in *2015 International Conference on Wireless Networks and Mobile Communications (WINCOM)*, pp. 1–6, Marrakech, Morocco, 2015.

[7] X. Yue, Y. Liu, S. Kang, A. Nallanathan, and Z. Ding, "Exploiting full/half-duplex user relaying in NOMA systems," *IEEE Transactions on Communications*, vol. 66, pp. 560–575, 2018.

[8] S. M. R. Islam, N. Avazov, O. A. Dobre, and K.-s. Kwak, "Power-domain non-orthogonal multiple access (NOMA) in 5G systems: potentials and challenges," *IEEE Communications Surveys & Tutorials*, vol. 19, pp. 721–742, 2017.

[9] L. Zhang, J. Liu, M. Xiao, G. Wu, Y. C. Liang, and S. Li, "Performance analysis and optimization in downlink NOMA systems with cooperative full-duplex relaying," *IEEE Journal on Selected Areas in Communications*, vol. 35, no. 10, pp. 2398–2412, 2017.

[10] V. Aswathi and A. V. Babu, "Non-orthogonal multiple access in full-duplex-based coordinated direct and relay transmission (CDRT) system: performance analysis and optimization," *EURASIP Journal on Wireless Communications and Networking*, vol. 2020, no. 1, 2020.

[11] X. Yue, Y. Liu, S. Kang, A. Nallanathan, and Y. Chen, "Modeling and analysis of two-way relay non-orthogonal multiple access systems," *IEEE Transactions on Communications*, vol. 66, no. 9, pp. 3784–3796, 2018.

[12] M. K. Shukla, H. H. Nguyen, and O. J. Pandey, "Secrecy performance analysis of two-way relay non-orthogonal multiple access systems," *IEEE Access*, vol. 8, pp. 39502–39512, 2020.

[13] X. Wang, M. Jia, I. W.-H. Ho, Q. Guo, and F. C. M. Lau, "Exploiting full-duplex two-way relay cooperative non-orthogonal multiple access," *IEEE Transactions on Communications*, vol. 67, pp. 2716–2729, 2018.

[14] N. Yang, P. L. Yeoh, M. Elkashlan, I. B. Collings, and Z. Chen, "Two-way relaying with multi-antenna sources: beamforming and antenna selection," *IEEE Transactions on Vehicular Technology*, vol. 61, no. 9, pp. 3996–4008, 2012.

[15] Y. Li, Y. Li, X. Chu, Y. Ye, and H. Zhang, "Performance analysis of relay selection in cooperative NOMA networks," *IEEE Communications Letters*, vol. 23, no. 4, pp. 760–763, 2019.

[16] T. N. Nguyen, P. T. Tran, and M. Voznak, "Wireless energy harvesting meets receiver diversity: a successful approach for two-way half-duplex relay networks over block Rayleigh fading channel," *Computer Networks*, vol. 172, article 107176, 2020.

[17] X. Yang, Z. Wang, X. Wan, and Z. Fan, "Secure energy-efficient resource allocation algorithm of massive MIMO system with SWIPT," *Electronics*, vol. 9, no. 1, p. 26, 2020.

[18] Y. Al-Eryani, M. Akrout, and E. Hossain, "Simultaneous energy harvesting and information transmission in a MIMO full-duplex system: a machine learning-based design," 2020, https://arxiv.org/abs/2002.06193.

[19] A. A. Nasir, X. Zhou, S. Durrani, and R. A. Kennedy, "Wireless-powered relays in cooperative communications: time-switching relaying protocols and throughput analysis," *IEEE Transactions on Communications*, vol. 63, no. 5, pp. 1607–1622, 2015.

[20] D. S. Gurjar and A. Das, "Wireless information and power transfer in three-phase two-way DF-relay networks over Nakagami-m fading," in *2019 IEEE VTS Asia Pacific Wireless Communications Symposium (APWCS)*, pp. 1–5, Singapore, 2019.

[21] J. Men, J. Ge, C. Zhang, and J. Li, "Joint optimal power allocation and relay selection scheme in energy harvesting asymmetric two-way relaying system," *IET Communications*, vol. 9, no. 11, pp. 1421–1426, 2015.

[22] G. Du, K. Xiong, Y. Zhang, and Z. Qiu, "Outage analysis and optimization for time switching-based two-way relaying with energy harvesting relay node," 2014, https://arxiv.org/abs/1412.7785.

[23] C. Peng, F. Li, and H. Liu, "Optimal power splitting in two-way decode-and-forward relay networks," *IEEE Communications Letters*, vol. 21, no. 9, pp. 2009–2012, 2017.

[24] W. Wu, B. Wang, Y. Zeng, H. Zhang, Z. Yang, and Z. Deng, "Robust secure beamforming for wireless powered full-duplex systems with self-energy recycling," *IEEE Transactions on Vehicular Technology*, vol. 66, no. 11, pp. 10055–10069, 2017.

[25] M. Aslam Chaudhry and S. M. Zubair, "Generalized incomplete gamma functions with applications," *Journal of Computational and Applied Mathematics*, vol. 55, no. 1, pp. 99–124, 1994.

[26] I. S. Gradshteyn I. M. Ryzhik et al., *Table of Integrals, Series and Products*, Academic, San Diego, CA, USA, 7th edition, 2007.